Circumnuclear Star Forming Activity in NGC 3982 *

Shui-Nai Zhang, Qiu-Sheng Gu and Yi-Peng Wang

Department of Astronomy, Nanjing University, Nanjing 210093, China; *snzhang@nju.edu.cn*

Abstract We present a study of the nearby Seyfert galaxy NGC 3982 using optical, infrared and X-ray data acquired by SDSS, Spitzer and Chandra. Our main results are as follows: (1) A simple stellar population synthesis on the nuclear and circumnuclear SDSS spectra gives unambiguous evidence of young stellar components in both the nuclear and circumnuclear regions. (2) The Spitzer Infrared Spectrograph (IRS) spectrum of the central region ($\sim 3''$) shows a power-law continuum, a silicate emission feature at $9.7\,\mu$m, and significant PAH emission features at 7.7, 8.6, 11.3 and $12.7\,\mu$m, suggesting the coexistence of AGN and starburst activities in the central region of NGC 3982. (3) We estimate the star formation rate (SFR) of the circumnuclear ($\sim 5'' - 20''$) region from the Hα luminosity to be $\mathrm{SFR}_{\mathrm{H}\alpha} = 0.52\,M_\odot\,\mathrm{yr}^{-1}$, which is consistent with the result from the Spitzer IRAC $8\,\mu$m luminosity, $\mathrm{SFR}_{8.0\,\mu\mathrm{m}} = 0.57\,M_\odot\,\mathrm{yr}^{-1}$. (4) We measure the spectral energy distribution for the active nucleus of NGC 3982 from radio to X-ray, and obtain a bolometric luminosity of $L_{\mathrm{bol}} = 4.5 \times 10^{42}$ erg s^{-1}, corresponding to an Eddington ratio ($L_{\mathrm{bol}}/L_{\mathrm{Edd}}$) of 0.014. The HST image of NGC 3982 shows a nuclear mini-spiral between the circumnuclear star-forming region and the nucleus, which could be the channel through which gas is transported to the supermassive black hole from the circumnuclear star-forming region.

Key words: galaxies: Seyfert — galaxies: starburst — galaxies: nuclei — galaxies: individual (NGC 3982)

1 INTRODUCTION

The connection between starburst and AGNs is one of the most important and hotly debated issues in the study of active galaxies. The recent discovery of a tight correlation between bulge stellar velocity and central black hole mass (Gebhardt et al. 2000; Ferrarese & Merritt 2000) suggests that a supermassive black hole is ubiquitous in all, or almost all, galaxies; and that the creation of these black holes is an integral part of the formation of galaxies. Thus, it is obvious that studies of galaxies with both starburst and AGN activities will greatly improve our understanding of the "starburst-AGN connection".

There is much observational evidence that many nearby active galaxies show circum-nuclear star-forming activities (González-Delgado & Perez 1993; Knapen et al. 2006; Simões Lopes et al. 2007). The general scenario of triggering starburst and AGNs activities is that the gas in the disk is channeled and accumulated towards the nuclear region by an axis-asymmetric potential, such as a bar (Huntley et al. 1978) or a galaxy-galaxy interaction (Combes 1998), or even a recent minor merger (Knapen et al. 2004; Mazzuca et al. 2006). Recent high-resolution HST observations of NGC 6951 and NGC 1097 show clear evidence that gas is transported to the nuclear starburst and super massive black hole (Fathi et al. 2006; Storchi-Bergmann et al. 2007).

NGC 3982 is just such a good example, that shows both circumnuclear star-forming activity and an active nucleus (Knapen et al. 2006). It is classified as Seyfert 1.9 by Ho et al. (1997) because of an extremely
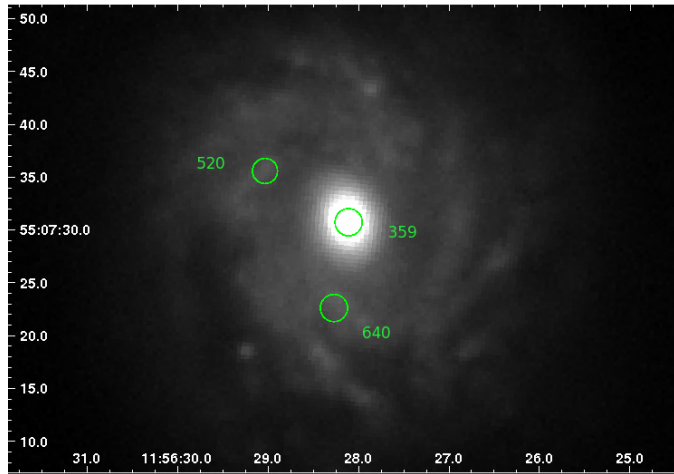
Fig. 1 SDSS i-band image of NGC 3982, where open circles mark the positions of three fibers.

faint broad Hα emission component. González-Delgado & Perez (1993) used the 4.2 m William Herschel Telescope on the La Palma mountain to observe the Hα image, and pointed out that the circum-nuclear ($\sim 5'' - 20''$) Hα emission is associated with a recent episode of star formation and they estimated the number of HII regions per square kpc to be 128. Bonatto et al. (1998) detected very blue UV spectra with the IUE data, illuminating the strong star formation activity. However, due to the large IUE aperture ($\sim 0.6\,\mathrm{kpc} \times 1.2\,\mathrm{kpc}$), it is impossible to disentangle the star-forming patchy ring (about 1 kpc) from the active nucleus. Sarzi et al. (2005) obtained a blue spectrum of the nuclear region of NGC 3982 acquired with the STIS on board HST. The aperture that extracted the spectrum of NGC 3982 has a size $0.2'' \times 0.25''$, which is equivalent in area to a circular aperture of radius $r = 0.13''$, corresponding to ~ 11 pc for the distance of 17.0 Mpc for NGC 3982 (Tully 1988). Using a simple stellar population synthesis, Sarzi et al. (2005) derived stellar contributions of 38.7% and 61.3% for stellar ages 10^7 and 3×10^9 yr, respectively. Due to the presence of strong high-excitation emission lines, the authors concluded that a power-law AGN component, rather than a young star population, is strictly needed in NGC 3982.

In this paper, we revisit the circumnuclear starburst and central AGN activities in NGC3982 using multi-wavelength data acquired with the Sloan Digital Sky Survey (SDSS), Spitzer and Chandra. This paper is organized as follows. In Section 2 we describe the multi-wavelength data reduction, and in Section 3 we present our main results. We discuss these results in Section 4 and draw our conclusions in Section 5. By using the WMAP data, Spergel et al. (2007) have well determined the cosmological constants of $H_0 = 73\,\mathrm{km\,s^{-1}\,Mpc^{-1}}$, $\Omega_\Lambda = 0.72$ and $\Omega_m = 0.24$, which will be used throughout this paper.

2 DATA REDUCTION

2.1 SDSS

Optical spectra are extracted from SDSS. There are three spectroscopic observations of NGC 3982, one (Fiber ID: 359) was centered on the nucleus of NGC 3982, the other two (Fiber ID: 520 and 640), on the circumnuclear star-forming regions. Figure 1 shows the SDSS i-band image of NGC 3982, where we also marked three fiber positions with open circles. In Table 1, we list the SDSS fiber ID, the position of fiber and the redshift derived from the emission lines. The fiber size is 3.0 arcsec and the spectral coverage is from 3800Å to 9170Å. These optical spectra have been corrected for Galactic reddening of $A(V) = 0.047$ by the standard IRAF [1] procedure. For convenience, the spectra are named by their fiber IDs throughout this paper.

---

[1] IRAF is distributed by the National Optical Astronomy Observatories, which are operated by the Association of Universities for Research in Astronomy, Inc., under cooperative agreement with the National Science Foundation.

Table 1 SDSS fiber ID, Position of fibers and Redshift derived from the Emission Lines.

Fiber ID	Object Name	RA	DEC	Redshift
359	SDSS J115628.12+550730.8	179.11720412	55.12523806	0.0040
520	SDSS J115629.02+550735.6	179.12095063	55.12657705	0.0039
640	SDSS J115628.22+550723.1	179.11760989	55.12310091	0.0043

2.2 Spitzer

The IRAC Basic Calibrated Data (BCD) of NGC 3982 were downloaded from the archive database of the Spitzer Science Center (SSC) through the program PID 3269 (the PI is Jack Gallimore). We reprocessed all the data from the BCD images, performing dark subtraction, detector linearization corrections, flat-field corrections, and flux calibrations (see also the IRAC Data Handbook [2]). The final mosaic images were obtained using custom-made IDL software (Huang et al. 2004). The absolute flux calibration of the IRAC bands have accuracy of better than 10% (Fazio et al. 2004). Throughout this paper, the magnitudes and colors are given in the AB system.

NGC 3982 was also observed in the spectral mapping mode with the Spitzer IRS using short, low resolution module (SL1: 7.4–14.5 μm and SL2: 5.2–7.7 μm). The exposure time per slit was 6.29 s. The pipeline BCD products from the SSC were downloaded, and bad, hot and rogue pixels were cleaned with an interactive IDL tool, IRSCLEAN_MASK, and then processed with the SMART software package (version 6.2.5, Higdon et al. 2004). The nuclear spectrum was extracted using an aperture of radius $r = 2.7''$ after subtracting the outmost image (about $20''$ away from the center) as background.

2.3 Chandra

NGC3982 was observed by ACIS-S onboard Chandra for a net exposure time of about 10.15 ks, which has a high resolution of $0.5''$ in the image. Data were reduced with CIAO (version 3.2) and the flux was estimated using XSpec (version 12.2). The source spectrum was extracted from a circular region with radius $2.2''$, while the background spectrum from a source-free, $60'' \times 35''$ rectangle. The spectra were binned to a minimum of 15 counts per bin in order to use the χ^2 statistics. Then the spectrum was fitted with a simple power-law model plus Galactic neutral absorption towards this target with column density fixed at $N_{\mathrm{H}} = 1.23 \times 10^{20} \, \mathrm{cm}^{-2}$ (Ghosh et al. 2007).

2.4 VLA

The radio continuum observation data at 5 GHz and 8 GHz were taken from VLA archive project AS806 (PI are Schmitt et al.), which were carried out with a configuration of VLA during 2004 September. The data reduction was kindly conducted by Fan Liu for us with the standard tasks of AIPS package.

## 3 RESULTS

3.1 Optical

In the SDSS spectra, we can clearly see the high-order Balmer absorption lines and weak absorption lines of Ca II K, G-band and Mg Ib. See Figure 2. We study the stellar population of the circum-nuclear and nuclear regions of NGC 3982 using the modified version of the stellar population synthesis code, *STARLIGHT* (version 4.0, Cid Fernandes et al. 2004), which adopted the new stellar library from Bruzual & Charlot (2003). The code synthesizes a given observed spectrum by a linear combination of Simple Stellar Populations (SSP). The spectrum is normalized at 4020 Å and the S/N ratio is measured in the window between 4730 and 4780 Å. Masks of 20~30 Å around the obvious emission lines are constructed, and more weights are given to the strongest stellar absorption features of Ca II K λ 3934, the G-band ($\sim$ 4300 Å), the Mg Ibλ 5173, and the Ca III triplets, that are less affected by nearby emission lines. An additional $f_\nu \sim \nu^{-1.5}$ power-law component is used to account for the contribution from AGN continuum emission (Watanabe et al. 2003).

After subtracting the synthetic stellar components (the solid lines in Fig. 2), we obtain the clean pure emission-line spectra (Fig. 3), where we can measure the accurate fluxes listed in Table 2. The main results of the spectral population synthesis are summarized as follows:

---

[2] *http://ssc.spitzer.caltech.edu/irac/dh/*
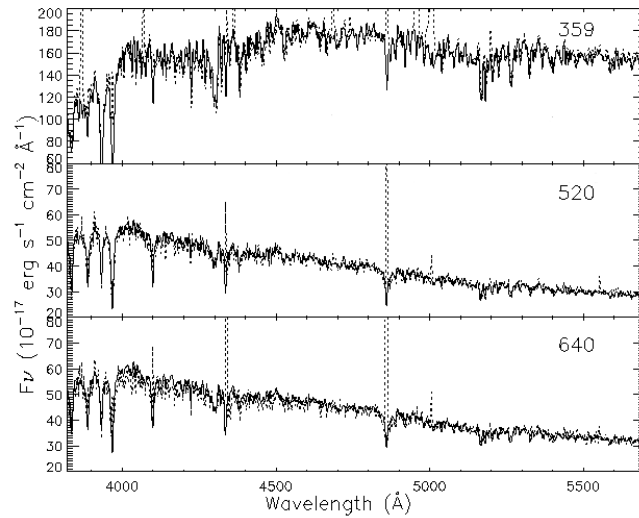
Fig. 2 Three SDSS spectra of NGC 3982. The solid lines represent the synthesized spectra, and the dotted lines, the observed spectra. The labels on the upper right of each panel are the fiber ID.
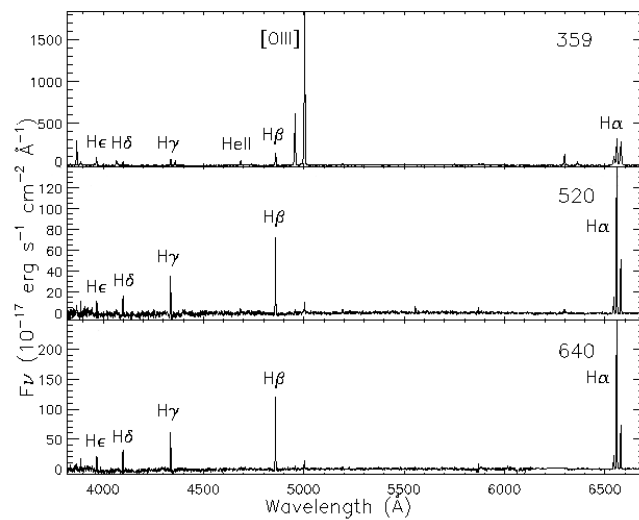
Fig. 3 Pure emission-line spectra of NGC 3982.

For No. 359 (the nucleus): about 7% of the total light at the normalized wavelength is contributed by a power-law featureless continuum, which can be attributed to AGN emission. There is 4% contribution from $3-5$ Myr young stellar population and 89% contribution from old stellar population (more than 1 Gyr).

For No. 520: 54% of total light is contributed by a young (less than 10 Myr) stellar population. The remaining 46% is from an old (> 1 Gyr) stellar component.

For No. 640: The stellar population is very similar to that of No. 520. About 57% light is from a young (less than 40 Myr) stellar population and 43% from an old (> 1 Gyr) stellar population.

Table 2 Absorption and Emission Lines

Center	Ion	Flux[a]	Eqw[a]	Flux[b]	Eqw[b]	Flux[c]	Eqw[c]
3835	H9	708.9	6.645	213.9	4.188	217.6	3.968
3889	H8	178.9	1.680	237.1	4.393	217.9	3.837
3933	CaIIK	800.6	6.717	193.3	3.569	207.6	3.634
3970	Hϵ	854.9	6.828	336.6	6.251	331.5	5.793
4101	Hδ	360.9	2.351	173.8	3.333	177.8	3.137
4300	G band	1129	7.011	166.8	3.432	204.1	3.863
4340	Hγ	293.1	1.817	137.9	2.907	132.4	2.572
4340[e]	Hγ	351.8	/	159.0	/	260.8	/
4363[e]	[OIII]	219.4	/	/	/	/	/
4686[e]	HeII	254.7	/	/	/	/	/
4861[e]	Hβ	660.6	/	293.2	/	498.0	/
4959[e]	[OIII]	2948	/	24.89	/	25.76	/
5007[e]	[OIII]	8731	/	45.05	/	74.93	/
5173	MgIb	502.8	/	86.07	/	93.05	/
5893	NaID	335.5	2.373	49.77	1.859	58.28	1.942
6548[e]	[NII]	652.6	/	118.8	/	171.8	/
6563[e]	Hα	1970	/	845.4	/	1436	/
6583[e]	[NII]	1752	/	315.5	/	416.9	/
6716[e]	[SII]	447.1	/	126.6	/	154.4	/
6731[e]	[SII]	574.9	/	89.01	/	105.1	/

[a], [b], [c] for the spectra 359, 520, 640 respectively, and [e] for emission lines. Observed flux is in unit of 10^{-17} erg s^{-1} cm^{-2}.
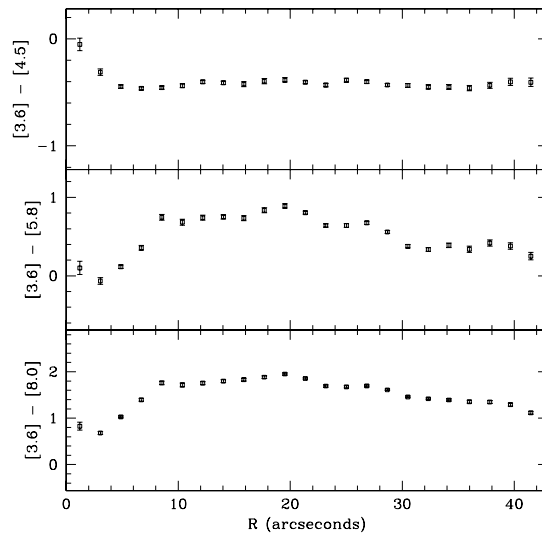
3.2 Infrared

IR surface photometry was performed on the IRAC images, using the *ellipse* program in the ISOPHOT package of IRAF. In order to match the PSFs of the four IRAC bands, we used the convolution kernels provided by Karl Gordon [3] to dilute the 3.6, 4.5 and 5.8 μm IRAC images so that they have the same spatial resolution as the 8.0 μm image. Following Gu et al. (2007), we first measure the 3.6 μm image where the Signal-to-Noise (S/N) ratio is the highest. The isophotal parameters, such as ellipticity and position angle, are kept. We then applied the surface photometry on the 4.5, 5.8 and 8.0 μm images. NGC3982 is an extended source, so the IRAC photometry calibration designed for point sources is not suitable. We adopt an additional aperture correction provided by Tom Jarrett [4] for extended sources, for the photometry. We then obtained accurate IRAC color distributions for NGC 3982.

Figure 4 shows the three IRAC color profiles, [3.6]–[4.5], [3.6]–[5.8], and [3.6]–[8.0] of NGC 3982. The central region in the [3.6]–[4.5] profile shows a much redder color which is responsible for the IR emission from AGN (Gu et al. 2007). In the [3.6]–[5.8] and [3.6]–[8.0] profiles, a clear "bump" exists at $10'' < R < 20''$ where the circumnuclear ring lies, indicating star-forming activity. Especially, the color [3.6]–[8.0] is stronger than in a normal T3 type galaxy (Pahre et al. 2004). This is because star formation increases the ratio of polycyclic aromatic hydrocarbon (PAH) emission at 8.0 μm to stellar mass at 3.6 μm (Gillett et al. 1973).
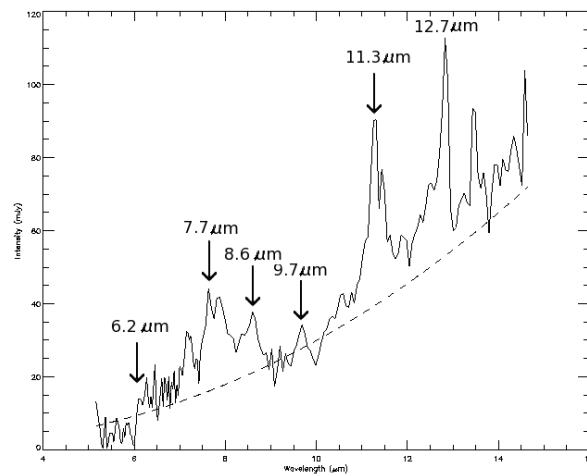
The IRS spectrum of the nuclear regions of NGC 3982 is shown in Figure 5. It is well known that PAH emission features are very weak or even absent in AGNs, as their carriers could be easily destroyed by the AGNs' strong UV emission (Genzel et al. 1998; Rigopoulou et al 1999). However, in the IRS spectrum of the central region ($R \sim 2.7''$) of NGC 3982 (Fig. 5), we clearly detect strong PAHs emission (6.2, 7.7, 8.6, 11.3 and 12.7 μm) superimposed on a power-law continuum. The dashed line represents a typical Seyfert 2 IR continuum with power-law index –2.3 (Catherine et al. 2006). As we know, PAH emission features are a good tracer of star formation activity (Peeters et al. 2004; Wu et al. 2005), so there must be star-forming activity in the central $\sim 3''$ region of NGC 3982. This is consistent with our stellar population synthesis of the SDSS nuclear spectrum. Although the 7.7 μm feature is the strongest PAH emission, it is contaminated by the 8.6 μm feature and so is difficult to measure accurately (Y. Shi, private communication). Shi et al. (2007) suggested that the 11.3 PAH feature is a much better tracer of star formation rate. We measured

---

[3] *http://dirty.as.arizona.edu/ kgordon/mips/conv_psfs/conv_psfs.html*

[4] *http://spider.ipac.caltech.edu/staff/jarrett/irac/calibration/index.html*

Fig. 4 IRAC color distribution for NGC 3982.

Fig. 5 Spitzer IRS spectrum of NGC 3982, taken from the central region ($<$ 220 pc). The dashed line represents a power-law continuum of index –2.3.

the flux of 11.3 μm PAH emission to be 3.28×10^{-13} erg cm^{-2} s^{-1}, corresponding to a luminosity of $2.9 \times 10^6 L_\odot$.

3.3 X-ray

There is a point-like source in the center of the Chandra X-ray image of NGC 3982, suggesting the presence of a central AGN. However, due to the short observing time and the low S/N, only the flux of soft X-ray (0.5–2 keV) could be obtained, which amounted to 2.0×10^{-14} erg cm^{-2} s^{-1}, similar to that ($\sim 1.8 \times 10^{-14}$ erg cm^{-2} s^{-1}) estimated from the XMM-Newton image by Guainazzi et al. (2005). The model gives

a best-fit value of $\Gamma = 3.2 \pm 0.5$. Here $\chi^2 \sim 3.8$ does not indicate a good fit, but the other models can not constrain any of the fit parameters (Ghosh et al. 2007).

3.4 Radio

The final cleaned maps at 5GHz and 8GHz, respectively have beam FWHMs of $0.62'' \times 0.42''$ and $0.35'' \times 0.30''$, and rms noises of $17.3\,\mu$Jy and $13.04\,\mu$Jy. We used a 2-D Gaussian function to fit the nuclear distribution and estimate the flux. The flux for the nuclear region at 5 GHz is 1.343×10^{-3} Jy and, at 8 GHz, is 1.807×10^{-3} Jy.

4 DISCUSSION

4.1 Patchy Star-Forming Ring

NGC 3982 is known to show a circumnuclear star-forming, patchy ring from $5''$ to $20''$, as indicated by the Hα observations (González-Delgado & Perez 1993). Our stellar population synthesis on the SDSS spectra of the circumnuclear region ($9''$ from the center) shows clearly that the recent ($\sim 10^7$ yr) star-forming activity contributes more than 50% of the light in the circumnuclear region of NGC 3982.

The intrinsic nebular extinction could be estimated from the observed Balmer decrement (Vacca & Conti 1992). From the pure emission-line spectra of the nucleus and two star-forming regions of NGC 3982, we measured the Balmer decrement (H$_\alpha$/H$_\beta$) to be 2.99, 3.11 and 3.12, respectively. We find that there is no obscuration for the nucleus (No. 359), while the intrinsic E_{B-V} for the two star-forming regions (Nos. 520 and 640) is 0.08. The fluxes and equivalent widths of the absorption and emission lines are listed in Table 2, where the emission lines have been corrected for intrinsic nebular extinction. From the ratio of [SII]$\lambda\lambda$ 6716/6730, we could derive the electron density in the ring to be about a few times $10\,\mathrm{cm}^{-3}$, assuming an electron temperature of 10^4 K (Osterbrock & Ferland 2005).

An average Hα flux is obtained from the spectrophotometric observations of two star-forming regions (Nos. 520 and 640) of NGC 3982. While from the Hα observation by González-Delgado & Perez (1993), we know that the star-forming ring lies between two ellipsis with semi-major axes of $5''$ and $20''$, and an inclination of $29°$, as shown in Figure 6. Since the star formation rate (SFR) is not uniform, it is difficult to estimate the Hα flux for the whole ring region. Of the SDSS r-band image, we measured the surface brightness of both the ring region and two circular regions of radius of $1.5''$ centered on the fibers Nos. 520 and 640, to derive a correcting factor. By multiplying the factor, the Hα flux could be extended to the whole circumnuclear region, to the value,

$$F(\mathrm{H}\alpha) = 5.36 \times 10^{-13}\,\mathrm{erg\ cm}^{-2}\,\mathrm{s}^{-1}.$$

Thus the SFR in the ring is (Calzetti et al. 2007)

$$\mathrm{SFR}(\mathrm{H}\alpha) = 5.3 \times 10^{-42}\,L(\mathrm{H}\alpha) = 0.52\,M_\odot\,\mathrm{yr}^{-1}.$$

For comparison, we also estimated the SFR from the pure dust 8 μm flux after removing the stellar emission using the 3.6 μm image (Wu et al. 2005). See Figure 6. The total flux of 8 μm from the same ring region is

$$F(8\,\mu\mathrm{m}) = 2.62 \times 10^{-24}\,\mathrm{erg\ s}^{-1},$$

and the corresponding SFR is (Wu et al. 2005):

$$\mathrm{SFR}(8\,\mu\mathrm{m}) = \frac{\nu\,L\nu[8\,\mu\mathrm{m}]}{1.57 \times 10^9\,L_\odot} = 0.57 M_\odot\,\mathrm{yr}^{-1}.$$

It is interesting to note that SFRs estimated from Hα and 8.0 μm are consistent.

4.2 The Nucleus

From the pure emission-line spectrum of the nucleus (No. 359), we derived $\log([\mathrm{OIII}]\lambda5007/\mathrm{H}\beta) = 1.121$ and $\log([\mathrm{NII}]\lambda6583/\mathrm{H}\alpha) = -0.051$, which is consistent with the Seyfert 2 classification of NGC 3982 (Véron-Cetty & Véron 2000) based on the BPT diagrams (Baldwin, Phillips & Terlevich 1981).
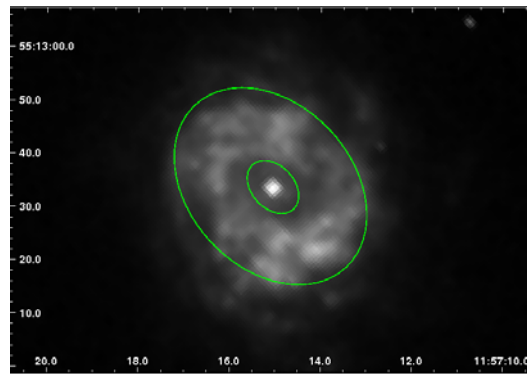
Fig. 6 Spitzer IRAC 8 μm image of NGC 3982, after removal of the stellar contribution. The SFR is calculated for the ring region between the two ellipses with semi-major axes of $5''$ and $20''$.
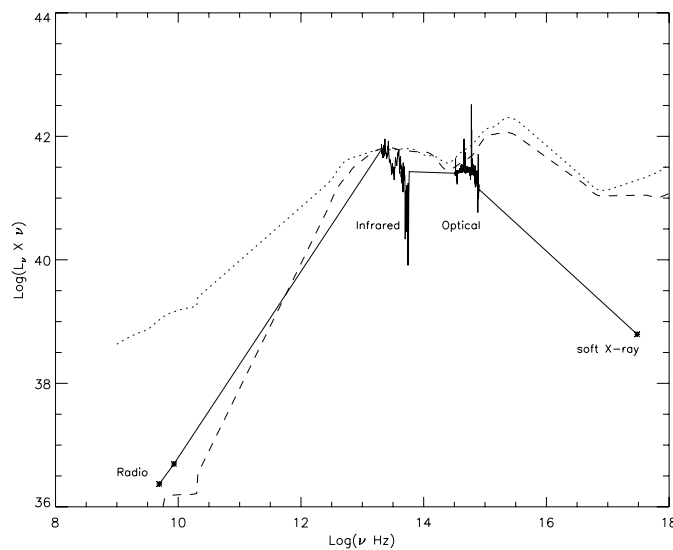
Fig. 7 SED of NGC 3982. The dotted line is a typical curve for radio loud AGN, and the dashed line is the one for radio quiet AGN (Elvis et al. 1994).

Using a direct-fit method in the pixel domain, Barth et al. (2002) obtained the velocity dispersion of NGC 3982 to be $\sigma = 73 \pm 4 \, \mathrm{km \, s^{-1}}$. Thus the black hole mass is

$$M_{\mathrm{BH}} = 10^{8.13} \, (\sigma/200 \, \mathrm{km \, s^{-1}})^{4.02} \, M_\odot = 2.35 \times 10^6 \, M_\odot$$

(Tremaine et al. 2002). The corresponding Eddington luminosity is $3.25 \times 10^{44} \, \mathrm{erg \, s^{-1}}$.

Combining all available multi-wavelength data of the nuclear region of NGC 3982 extending from radio, infrared and optical to X-ray, we derived the Spectral Energy Distribution (SED) of NGC 3982 shown in Figure 7. A comparison with the spectra of typical radio-loud and radio-quiet AGN (Elvis et al. 1994) suggests that NGC3982 is a radio-quiet AGN. However, the X-ray flux is much lower, which might be due to the Compton-thick absorption (Shu et al. 2007). Integrating the SED of NGC 3982, we obtain a bolometric luminosity of $4.5 \times 10^{42} \, \mathrm{erg \, cm^{-2} \, s^{-1}}$, which is about 1.4% the Eddington luminosity, a typical value for Seyfert 2 galaxies (Panessa et al. 2006).

It was thought that it might be difficult to form stars in the very central regions of AGNs, because the black hole may disrupt any molecular clouds before their gravitational collapse starts. However, some observations have shown that young stellar clusters can coexist with super massive black holes on very small scales, at least in some Seyfert 2 and LINER nuclei (Heckman et al. 1997; Colina et al. 2002). Based on the STIS spectrum of the nuclear region ($\sim 0.13''$) of NGC 3982, Sarzi et al. (2005) were inclined to the view that there was no young star population in its central region. Our results of simple stellar population of the nuclear ($r = 1.5''$) spectrum indicate about 4% of young stars, with age similar to that of the star-forming ring. The presence of young stellar population is also confirmed by the strong PAH emission features in the Spitzer IRS spectrum. We should carefully note the aperture sizes of STIS, SDSS and IRS: they are, respectively, $0.13''$, $1.5''$ and $2.7''$. It is probable that the young stellar population is located between $0.13''$ and $2.7''$.

Using the converting factor provided by Yong Shi (private communication, see also Shi et al. 2007 for a detail), we estimated the far-infrared (8–1000 μm) emission contributed by star formation, from the $11.3\,\mu$m PAH feature (Section 3.2), to be $L_{\mathrm{FIR}} = 2.14 \times 10^8\,L_\odot$. Thus the SFR of the nuclear region is (Devereux & Young 1991),

$$\mathrm{SFR}(L_{\mathrm{FIR}}) = 1.4 \times 10^{-10}\,L_{\mathrm{FIR}} = 0.03\,M_\odot\,\mathrm{yr}^{-1}.$$
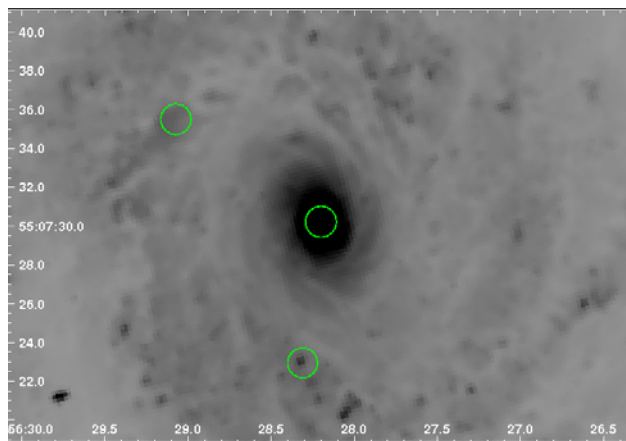
Fig. 8 In V-band HST image, the nuclear spiral can be seen clearly. The three circles are at the same positions as in Fig. 2.1.

4.3 Triggering Mechanism of Starburst and AGNs

The outstanding problem in the study of starburst and AGN activities is to know how the gas in the disk is channeled to the nuclear region. It is generally believed that an axis-asymmetric potential, such as due to a bar and galaxy-galaxy interaction, or even a recent minor merger can promote an efficient gas inflow (Huang et al. 1996; Ho, Filippenko & Sargent 1997; Englmaier & Shlosman 2004; Huntley et al. 1978; Combes 1998; Knapen et al. 2004; Mazzuca et al. 2006). On the basis of a large sample of HST images, Martini & Pogge (1999), Martini et al. (2003) and Hunt & Malkan (2004) estimated that nuclear spirals reside in about 50% of the active galaxies, and are responsible for fuelling the central AGN activity. Storchi-Bergmann et al. (2007) presented clear evidence of gas streaming motions along nuclear spiral arms towards the LINER nucleus of NGC 6951.

NGC 3982 is cataloged as an SAB(r)b galaxy in NED [5], therefore we believe that the circumnuclear star-forming activity is triggered by bar-induced gas inflow. On checking the high-resolution HST image (Fig. 8), we do detect a nuclear spiral, which connects the circumnuclear region and the nucleus, which might be responsible for fueling the nuclear SMBH.

---

[5] *http://nedwww.ipac.caltech.edu/*

5 CONCLUSIONS

In this paper we investigate the nearby galaxy NGC 3982 using the multi-wavelength data obtained from SDSS, Spitzer and Chandra. We confirm that it is a typical Seyfert galaxy, and find coexistence of AGN and starburst activities in the central region ($< 2.7''$). The SFR of the circumnuclear region ($\sim 5'' - 20''$) is estimated to be $\mathrm{SFR}_{\mathrm{H}\alpha} = 0.52\ M_\odot\ \mathrm{yr}^{-1}$ from the Hα luminosity, and $\mathrm{SFR}_{8.0\,\mu\mathrm{m}} = 0.57\ M_\odot\ \mathrm{yr}^{-1}$ from the Spitzer IRAC $8\,\mu$m luminosity. A nuclear mini-spiral exists between the circumnuclear star-forming patchy ring and the nucleus, and may be responsible for fueling the supermassive black hole by transferring gas from the circumnuclear star-forming region.

References

Baldwin A., Phillips M. M., Terlevich R., 1981, PASP, 93, 5
Barth A. J., Ho L. C., Sargent W. L. W., 2002, AJ, 124, 2607
Bonatto C., Pastoriza M. G., Alloin D., Bica E., 1998, A&A, 334, 439
Bruzual G., Charlot S., 2003, MNRAS, 344, 1000
Catherine L. B., Jack F. G., Christopher P. O. et al., 2006, AJ, 132, 401
Calzetti D., Kennicutt R. C., Engelbrache C. W. et al., 2007, ApJ, 666, 870
Cid Fernandes R., Gu Q., Melnick J. et al., 2004, MNRAS, 355, 273
Colina L., González-Delgado R., Mas-Hesse J. M., Leitherer C., 2002, ApJ, 579, 545
Combes F., 1998, IAUS, 184, 495
Devereux N. A., Young J. S., 1991, ApJ, 371, 515
Elvis M., Wilkes B. J., McDowell J. C. et al., 1994, ApJS, 95, 1
Englmaier P., Shlosman L., 2004, ApJ, 617, L115
Fathi K., Storchi-Bergmann T., Riffel R. A. et al., 2006, ApJ, 641, L25
Fazio G. G., Hora J. L., Allen L. E. et al., 2004, ApJS, 154, 10
Ferrarese L., Merritt D., 2000, ApJ, 539, L9
Gebhardt K., Bender R., Bower G. et al., 2000, ApJ, 539, L13
Genzel R., Lutz D., Sturm E. et al., 1998, ApJ, 498, 579
Gillett F. C., Forrest W. J., Merrill K. M., 1973, ApJ, 183, 87
Ghosh H., Pogge R. W., Mathur S., Martini P., Shields J. C., 2007, ApJ, 656, 105
González-Delgado R. M., Perez E., 1993, Ap&SS, 205,127
Gu Q.-S., Huang J.-S., Wilson G., Fazio G. G., 2007, ApJ, 671, L105
Guainazzi M., Matt G., Perola G. C., 2005, A&A, 444, 119
Heckman T. M., González-Delgado R., Leitherer C. et al., 1997, ApJ, 482, 114
Higdon S. J. U., Devost D., Higdon J. L. et al., 2004, PASP, 116, 975
Ho L. C., Filippenko A. V., Sargent W. L. W., 1997, ApJ, 487, 591
Ho L. C., Filippenko A. V., Sargent W. L. W., Peng, Chien Y., 1997, ApJS, 112, 391
Huang J.-H., Gu Q.-S., Su H.-J., Hawarden T. G., Liao X.-H., Wu G.-X., 1996, A&A, 313, 13
Huang J.-S., Barmby P., Fazio G. G. et al., 2004, ApJS, 154, 44
Hunt, L. K., Malkan, M. A., 2004, ApJ, 616, 707
Huntley J. M., Sanders R. H., Roberts W. W., 1978, ApJ, 221, 521
Knapen J. H., Whyte L. F., de Blok W. J. G., van der Hulst J. M., 2004, A&A, 423, 481
Knapen J. H., Mazzuca L. M., Böker T. et al., 2006, A&A, 448, 489
Martini P., Pogge R. W., 1999, AJ, 118, 2646

Martini, P., Regan M. W., Mulchaey J. S., Pogge R. W., 2003, ApJ, 589, 774

Mazzuca L.M., Sarzi M., Knapen J. H., Veilleux S., Swaters R., 2006, ApJ, 649, L79

Osterbrock D., Ferland G. J., 2005, Astrophyscis of Gaseous Nebulae and Active Galactic Nuclei–2nd ed, University Science Books

Panessa F., Bassani L., Cappi M. et al., 2006, A&A, 455, 173

Pahre M. A., Ashby M. L. N., Fazio G. G., Willner S. P., 2004, ApJS, 154, 235

Peeters E., Spoon H. W. W., Tielens A. G. G. M., 2004, ApJ, 613, 986

Rigopoulou D., Spoon H. W. W., Genzel R. et al., 1999, AJ, 118, 2625

Sarzi M., Rix H., Shields J. C. et al., 2005, ApJ, 628, 169

Shi Y., Ogle P., Rieke G. H. et al., 2007, ApJ, 669, 841

Shu X.-W., Wang J.-X., Jiang P., Fan L.-L., Wang T.-G., 2007, ApJ, 657, 167

Simões Lopes R. D., Storchi-Bergmann T., de Fátima Saraiva M., Martini P., 2007, ApJ, 655,718

Spergel D. N., Bean R., Doré O. et al., 2007, ApJS, 170, 377

Storchi-Bergmann T., Dors O. L. J., Riffel R. A. et al., 2007, 670, 959

Tremaine S., Gebhardt K., Bender R. et al., 2002, ApJ, 574, 740

Tully R. B., Nearby galaxies catalog, 1988, Cambridge and New York, Cambridge University Press

Vacca W. D., Conti P. S., 1992, ApJ, 401, 543

Véron-Cetty M. P., Véron P., 2000, A&A Rev., 10, 81

Watanabe M., Nagata T., Sato S., Nakaya H., Hough J. H., 2003, ApJ, 591, 714

Wu H., Cao C., Hao C.-N. et al., 2005, ApJ, 632, L79